

ChemComm

Accepted Manuscript



This is an *Accepted Manuscript*, which has been through the Royal Society of Chemistry peer review process and has been accepted for publication.

Accepted Manuscripts are published online shortly after acceptance, before technical editing, formatting and proof reading. Using this free service, authors can make their results available to the community, in citable form, before we publish the edited article. We will replace this *Accepted Manuscript* with the edited and formatted *Advance Article* as soon as it is available.

You can find more information about *Accepted Manuscripts* in the [Information for Authors](#).

Please note that technical editing may introduce minor changes to the text and/or graphics, which may alter content. The journal's standard [Terms & Conditions](#) and the [Ethical guidelines](#) still apply. In no event shall the Royal Society of Chemistry be held responsible for any errors or omissions in this *Accepted Manuscript* or any consequences arising from the use of any information it contains.

Journal Name

COMMUNICATION

Reversible Stimulus-Responsive Cu(I) Iodide Pyridine Coordination Polymer

 Received 00th January 20xx,
Accepted 00th January 20xx

 P. Amo-Ochoa,^{*a} K. Hassanein,^a C. J. Gómez-García,^b S. Benmansour,^b J. Perles,^c O. Castillo,^d J. I. Martínez,^e P. Ocón^f and F. Zamora^{*a,g}

DOI: 10.1039/x0xx00000x

www.rsc.org/

We present a structural flexible copper-iodide-pyridine based coordination polymer showing drastic variations in its electrical conductivity driven by temperature and sorption of acetic acid molecules. The dramatic effect on the electrical conductivity enables the fabrication of a simple and robust device for gas detection. X-ray diffraction studies and DFT calculations allow to rationalize these observations.

In recent years, coordination polymers (CPs) have gained increasing attention due to their wide structural variety and interesting physico-chemical properties.¹ They are a potential source of multifunctional materials that can bring remarkable physical properties such as luminescence,² non-linear optics,³ magnetism⁴ and electrical conductivity.⁵ CPs have the ability to produce dynamic structures due to the structural flexibility of the ligands and/or the ability of the coordination sites to exchange, release and/or re-accommodate molecules rendering CPs as a source of stimuli-responsive materials.⁶ These dynamic materials show potential applications as chemical switches, memories or molecular sensors. A limited number of CPs have shown spin-crossover transitions modulated or induced by a chemical stimulus such as gas or solvent sorption in the pores,^{7–11} magnetic physically-driven solid-state transformation,^{12, 13} Stimuli-responsive electrical

materials, mainly centred on organic conductive polymers,¹⁴ are of high current interest. A recent example of thin-film device based on the porous coordination polymer Cu₃(BTC)₂ (BTC = benzene-1,3,5-tricarboxylic acid) has shown electrical response to 7,7,8,8-tetracyanoquinodimethane (TCNQ) guest molecules.¹⁵ Quasi-linear physical properties have also been reported for MX and MMX chains (M = transition metal, X = halide) some of them showing thermal Peierls transitions that affect their magnetic properties¹⁶ and/or their electrical conductivity.¹⁷

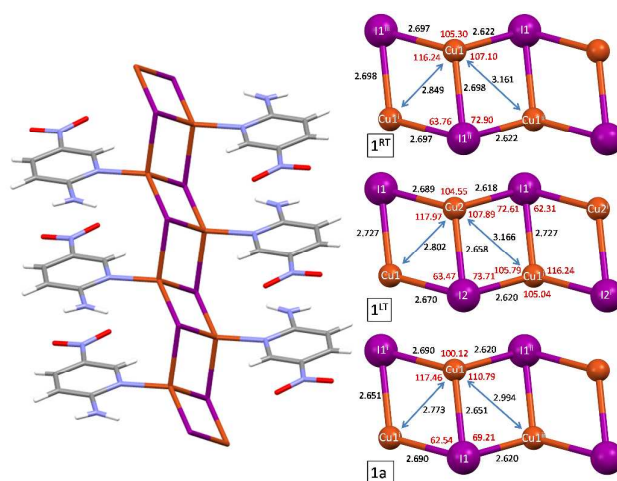


Figure 1. (left) View of the polymeric [Cu(C₅H₅N₃O₂)]_n chain in compounds **1** and **1a**. Colour code: orange(Cu), purple (I), grey (C), blue (N), red (O). (right) Fragment of the double-stranded stair in **1^{RT}**, **1^{LT}** and **1a** showing the bond angles (°) and distances (Å).

Additionally, we have reported that some double stranded Cu-halide stairs present interesting physical properties.¹⁸ Here we disclose two 1D-CP polymorphs of Cu(I) with iodide as bridging ligands and 2-amino-5-nitropyridine (C₅H₅N₃O₂, ANP) as terminal ligands showing very flexible structures enabling a reversible physically-driven electrical conductive transition with electrical bi-stability close to room temperature and a chemically-driven transition that induces a dramatic

^a Departamento de Química Inorgánica, Universidad Autónoma de Madrid, 28049 Madrid, Spain. E-mail: felix.zamora@uam.es

^b Instituto de Ciencia Molecular (ICMol), Parque Científico, Universidad de Valencia, Catedrático José Beltrán, 2. 46980 Paterna Valencia, Spain.

^c Servicio Interdepartamental de Investigación, Universidad Autónoma de Madrid, 28049 Madrid, Spain.

^d Departamento de Química Inorgánica, Universidad del País Vasco. Apartado 644, e-48080 Bilbao, Spain.

^e Instituto de Ciencia de Materiales CSIC, 28049 Madrid (Spain).

^f Departamento de Química Física Aplicada, Universidad Autónoma de Madrid, Madrid, Spain.

^g Condensed Matter Physics Center (IFIMAC), Universidad Autónoma de Madrid, 28049 Madrid, Spain.

† Footnotes relating to the title and/or authors should appear here.

Electronic Supplementary Information (ESI) available: Experimental details, Crystallographic data and structure refinement details of all the compounds, additional data of X-ray studies on thermal variation parameters of compound **1**, supramolecular interactions details and DFT calculations of **1^{LT}**, **1^{RT}** and **1a**, and additional data of the studies on the device characterization based on compound **1**, are free available. See DOI: 10.1039/x0xx00000x

enhancement of the electrical conductivity allowing the fabrication of a simple and robust gas detector device.

The direct reactions carried out between CuI and ANP at 25 °C or under solvothermal conditions lead to the isolation of $[\text{Cu}(\text{C}_5\text{H}_5\text{N}_3\text{O}_2)]_n$ (**1**) and its polymorph **1a**, respectively. **1a** is isostructural to the Br derivative, also prepared under solvothermal conditions.¹⁹ Both polymorphs show a double-stranded stair motif in which Cu(I) centres are bridged by μ_3 -I. Since the electrical properties (see below) of compound **1** indicate a phase transition at *ca.* 267–282 K, we have studied in detail the thermal dependence of the unit cell parameters of **1** (Figures S1–S6) and solved the structure of **1** at 200 K (**1^{LT}**) and at 298 K (**1^{RT}**). **1^{RT}**, **1^{LT}** and **1a** contain Cu(I) ions with a tetrahedral environment formed by three bridging iodine ions and the iminic nitrogen atom of the 2-amino-5-nitropyridine ligand (Figure 1).

Table 1. D.C. conductivity values at 300 K and experimental and calculated activation energies in compounds **1^{LT}**, **1^{RT}** and **1a**.

compound	$\sigma_{300\text{K}}$ (Scm^{-1})	E_g (eV) exp.	E_g (eV) calc.
1^{LT}	–	0.08	0.18
1^{RT}	1.1×10^{-8}	0.40	0.59
1a	5.0×10^{-6}	0.37	0.31

The Cu–I and Cu–N bond distances are similar to those found in similar $[\text{Cu}(\text{L})_n]$ stairs.^{20–26} The intra-chain Cu...Cu distances are close or below the sum of the van der Waals radii (2.80 Å). Interestingly, the Cu–I chain structure presents slight variations along the propagation direction (*a*), as shown by the unit cell *a* parameter (4.2284(1), 4.1982(1), and 4.0708(1) Å for **1^{RT}**, **1^{LT}** and **1a**, respectively) also reflected in the corresponding Cu–I–Cu and I–Cu–I bond angles along the chain (105.3° for **1^{RT}**, 104.5–105.0° for **1^{LT}** and 100.1° for **1a**) (Figure 1). Finally, the dihedral angle between adjacent Cu_2I_2 units along the chain also shows slight variations between both polymorphs (117.4° for **1^{RT}**, 117.3° and 116.8° for **1^{LT}** and 114.1° for **1a**). These differences observed mainly between polymorphs **1** and **1a** suggest that the inter-chain interactions are important in determining the overall structure of these compounds, supporting the idea that the ANP ligand plays a crucial structural role. The ANP ring is tilted (78.2° for **1^{RT}**, 79.0° for **1^{LT}** and 77.6° for **1a**) and twisted (57.4° for **1^{RT}**, 56.0° for **1^{LT}** and 67.1° for **1a**) relative to the propagation direction of the chain. The chain cohesion is also ensured by the presence of π – π stacking interactions at both sides of the chain between adjacent ANP ligands with interplanar distances of 3.332 Å (**1^{RT}**), 3.296 and 3.307 Å (**1^{LT}**) and 3.520 Å (**1a**). All compounds show weak intra-chain hydrogen bonds involving the halide as acceptor and the NH_2/CH groups as donors thanks to the twisting of the ANP ligands. The nitro substituent of the ANP ligand plays a key role assembling the chains together through hydrogen bonds between the NH_2 and C–H donor groups of neighbouring chains and the NO_2 group as an acceptor. However, although similar interactions are present in these compounds, the total number of hydrogen bonds involving the

ANP ligands differs (Figure S7). The order of hydrogen bond connectivity is **1^{RT}** < **1^{LT}** < **1a**. Interestingly, the average intra-chain Cu...Cu distances are shorter in the dimerised phase (**1^{LT}**) than in the regular one (**1^{RT}**) (Figure 1). **1a** shows intra-chain Cu...Cu distances shorter than **1^{LT}** and **1^{RT}**.

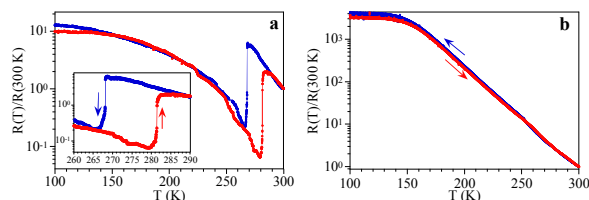


Figure 2. Thermal variation of the normalized resistance of compounds **1** (a) and **1a** (b) in two successive cooling and heating and scans (1 and 2, respectively) in the 100–300 K range. Inset in (a) shows the reversible transition taking place at 268–281 K. The saturation of the resistance at low temperatures in both compounds indicates that the resistance has reached the limit of our equipment ($5 \times 10^{-5} \Omega$).

Electrical conductivity measurements at 300 K (Table 1) show that the room temperature average DC conductivity values are strongly dependent on the structure, with $\sigma(\mathbf{1a}) > \sigma(\mathbf{1})$, suggesting that the main factors determining the conductivity must be the structural parameters in the chain as the average Cu...Cu distance (3.01 Å in **1^{RT}**, 2.98 Å in **1^{LT}** and 2.88 Å in **1a**) and the dihedral angle between adjacent Cu_2I_2 units, which is closer to 90° in **1a** (114.1°) than in **1^{RT}** (116.8–117.4°), resulting in a better orbital overlap in **1a**. Compound **1** presents a reversible semiconducting–semiconducting transition with an abrupt transition at *ca.* 267 K in the cooling scan and *ca.* 282 K in the heating one and a hysteresis of *ca.* 15 K (Figure 2a). Interestingly, this transition implies a decrease in the resistivity by a factor of *ca.* 30 when passing from high to low temperature. Although the sample remains semiconducting before and after the transition, the activation energy decreases from *ca.* 0.40 eV at high temperatures to *ca.* 0.08 eV at low temperatures. These values indicate that the low temperature phase is a better conductor and has a lower activation energy, in contrast with the usual behaviour observed in chain compounds, where the Peierls transitions imply a decrease of the resistivity and an increase of the energy gap in the low temperature phase.^{27–31} This unexpected result can be explained with the structural data obtained for **1^{RT}** and **1^{LT}** above and below the transition temperature. The main difference between **1^{RT}** and **1^{LT}** is the presence of two independent Cu and I atoms in **1^{LT}**, compared to only one in **1^{RT}** and **1a**, resulting in a dimerised chain in **1^{LT}**.

1^{LT} presents a more homogeneous distribution of the Cu–I bond distances, a shorter average Cu...Cu distance along the chain (Figure 1) and a smaller dihedral angle between Cu_2I_2 units, suggesting that this phase must be a better conductor, in agreement with the experimental results. **1** and **1a** show very similar behaviours except for the transition at *ca.* 267–282 K that is only observed in **1** (Figure 2b). Thus, **1a** shows an activation energy of 0.37 eV, but no transition (Figure 2b). Theoretical calculations show that the electronic structure yield minimum values of the transport gaps at Γ points ranging between 0.18 and 0.59 eV for all the CPs (Figure S8), in excellent agreement with the experimental data (Table 1).

These calculations³² also show that **1** behaves as a typical p-type semiconductor with the Fermi level very close to the valence band. The valence and conduction band orbital electron isodensities for **1**^{RT}, **1**^{LT} and **1a** (Figure S9) shows a continuous hybridization band mostly located along the Cu-I skeleton and a continuous orbital *side-to-side* hybridization formed between the ligands, indicating that the conduction takes place only along the chains. Increasing temperatures allow charge migration from the valence band towards the conduction one, as well as a temperature-induced overlap between both bands, increasing the carrier mobility and the electronic conduction along the chains.

The flexible structure of **1** and the presence of ligands with available donor and acceptor H-bonds groups, prompted us to study the influence of external chemical stimuli in this material. Thus, when a microcrystalline powder of **1** is immersed in glacial acetic acid, a sorption process takes place, the crystals change from yellow to orange and loose the crystallinity, becoming amorphous (Figure S10). Surprisingly, this change is reversible and when the acetic acid is removed and the sample is dried in air during several days, the crystals become yellow and recover the crystallinity (Figure S10).

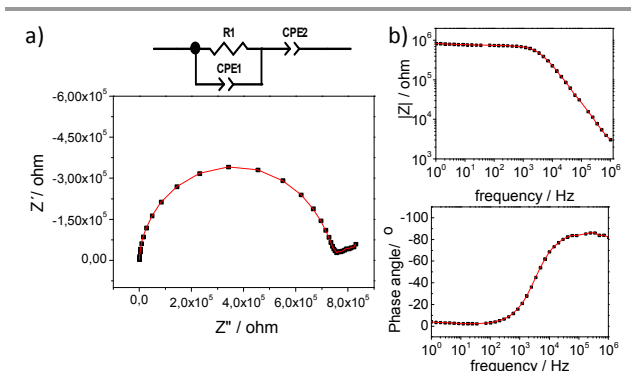


Figure 3. Nyquist plot and equivalent circuit (a) and Bode plot (b) of compound **1** after 24 h exposed to HAcO vapour. Experimental values (■), fitting values (-).

This reversible interaction has also been proven by the change in the electrical conductivity of **1**. Thus, Electrochemical Impedance Spectroscopy (EIS) measurements (Figure 3) on a device built with a pellet of **1** electrically contacted with two copper wires (Figure S11) showed a drastic reversible change in the conductivity when **1** is exposed to HAcO vapour after different exposure times. The Nyquist plot for compound **1**, after 24 h exposed to HAcO vapour, in the frequency range 1 Hz-1 MHz (Figure 3a) shows the presence of depressed semicircular arc at high-medium frequencies (1 MHz-30 Hz) that is attributed to the bulk properties of the compound and a line in the low frequency region typical of materials with capacitive behaviour occurring between the mobile ions (that are blocked by the electrode-electrolyte interphase).³³ The Nyquist plots recorded after different exposure times (45, 20 and 15 min) are similar to those obtained after 24 h exposure (Figures S12) but the intercept of the semicircle with the Z' axis shifts towards higher values. The pristine sample **1** ($t = 0$ min in HAcO vapour), loses the semicircle shape and, in addition, the

experimental measurements have a lot of dispersion from 100 Hz (Figure S12), suggesting that the material does not possess any inherent route for electrical conduction. The conductivity increases with increasing the exposure times to acetic acid vapours (Table S2) and reaches saturation after *ca.* 45 minutes of exposure. In agreement with the Bode diagram, the semicircle representing the bulk properties of compound **1** is shifted to higher frequencies when the HAcO exposure time increases. This fact indicates that the material/electrode interphase capacitive character becomes less important and the high conductive phase of **1** appears (Figure S12). When saturated acetic acid pellets were exposed to air (30 min. or longer times) the Nyquist plots lost the characteristics depressed semicircle shape and a poor value of conductivity is obtained (*ca.* 10^{-11} Scm^{-1}). If we compare those results with the experiments involving different exposure times in HAcO vapour, the behaviour clearly indicates the crucial role of the HAcO molecules in establishing the conductivity pathway. The geometric capacitance values obtained from the high-medium frequency region (1 MHz -30 Hz) are *ca.* 10^{-11} F and are independent of the HAcO exposure time. However the low frequency tail that could be assigned to the effect of electrode-electrolyte interactions and electrode polarization, gives capacitance values of 10^{-8} - 10^{-6} F. Albeit this value is dependent on the composition and hence can be attributed to interfacial phenomena. In order to check the reversibility and cycling capacity of the observed drastic change in the conductivity, after 12 h in air the sample was re-exposed to HAcO vapours for 3 h. The Nyquist plot and the conductivity value (*ca.* 10^{-6} Scm^{-1}) were similar to the first ones, confirming the total reversibility of the HAcO capture/release process and its effect on the conductivity of **1**. Successive on/off cycles (10 min in HAcO vapour followed by 70 min in air) yielded reproducible results (Figure 4) confirming the stability of the device. Furthermore, we have verified that after several weeks in air the device still presents the reproducible on/off cycles.

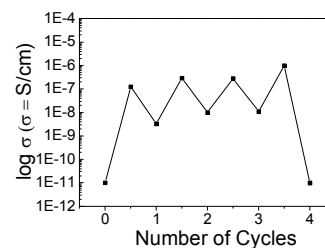


Figure 4. Conductivity variation vs on-off cycling of compound **1** at 298K.

In a separate experiment, a pellet of **1** was exposed to CH_3Cl vapour for 24 h at 298 K (Table S2). The EIS study at 298 K shows a conductivity of *ca.* 10^{-10} Scm^{-1} , indicating the poor influence of the chloroform vapours in contrast to the HAcO ones. This results agrees with the idea that CH_3Cl presents a much lower capacity to interact with the ANP ligands in **1** (it has no H-bonding capacity) and, accordingly, has a negligible ability to modify the structural parameters of the CuI chain. In contrast, HAcO has a high H-bonding capacity and, accordingly is expected to interact with the amino group of the ANP ligand

and to modify the structural parameters of the CuI chain, resulting in a drastic change of the conductivity value.

Finally, in order to check if the absorbed acetic acid molecules induce any relevant structural change in **1**, we have performed a powder X-ray diffraction study with a polycrystalline sample of **1** that was exposed to HAcO vapours during 24, 48 and 72 h. As expected, this study shows no dramatic structural changes in **1** upon HAcO absorption (powder X-ray diffractograms remain unchanged, Figures S13 and S14). This fact suggests that only a fraction of the sample becomes amorphous. Note that the capacity of HAcO molecules to interact with the ANP ligand and to slightly modify the CuI chain cannot be ruled out.

Conclusions

CuI double chain compounds with ANP as terminal ligand are very sensitive to external physical and chemical stimuli. We have prepared two polymorphs (**1** and **1a**), formulated as $[\text{Cu}(\text{C}_5\text{H}_5\text{N}_3\text{O}_2)]_n$, that allow a detailed study of the key role played by the structural parameters of the CuI chain in the electrical properties. Polymorph **1** shows a reversible thermally-induced transition with a hysteresis of ca. 15 K near room temperature that implies an unprecedented increase of a factor ca. 30 of the conductivity in the low temperature phase. This transition is due to slight reversible variations in the Cu/I bond distances and angles. The theoretical calculations suggest that the conduction mechanism seems to be produced along the one-dimensional chains exclusively. Furthermore, the extraordinary capacity of these chains to respond to chemical stimuli is exemplified by the behaviour observed in a device prepared with **1** that shows a reversible increase/decrease of the conductivity of ca. 4 orders of magnitude due to the uptake/release of HOAc in the structure. The high capacity of **1** to respond to external stimuli is attributed to two facts: i) the softness of the double CuI chains that renders these chains very dynamic and easy to distort, leading to huge changes in the electrical conductivity; and ii) the presence of ANP as terminal ligand directly connected to the CuI chains that acts as an antenna for the external chemical stimuli.

We thank support from MICINN (MAT2013-46753-C2-1-P, MAT2013-46502-C2-1/2-P and CTQ2011-26507), Eusko Jaurlaritza (S-PE13UN016) and Generalitat Valenciana (Prometeoil/2014/076). J.I.M. thanks CSIC-JAEDOC.

Notes and references

- S. R. Batten, S. M. Neville and D. Turner, *Coordination Polymers: Design, Analysis and Applications*, RSC Pub., 2009.
- Y. J. Cui, Y. F. Yue, G. D. Qian and B. L. Chen, *Chem. Rev.*, 2012, **112**, 1126-1162.
- C. Wang, T. Zhang and W. B. Lin, *Chem. Rev.*, 2012, **112**, 1084-1104.
- M. Kurmoo, *Chem. Soc. Rev.*, 2009, **38**, 1353-1379.
- G. Givaja, P. Amo-Ochoa, C. J. Gomez-Garcia and F. Zamora, *Chem. Soc. Rev.*, 2012, **41**, 115-147.
- See the recent themed issues on MOFs: (a) *Chem. Soc. Rev.* 2009, 1201-1508. (b) *Chem. Rev.* 2012, 112, 673-1268.
- M. C. Munoz and J. A. Real, *Coord. Chem. Rev.*, 2011, **255**, 2068-2093.
- J. Ferrando-Soria, P. Serra-Crespo, M. de Lange, J. Gascon, F. Kapteijn, M. Julve, J. Cano, F. Lloret, J. Pasan, C. Ruiz-Perez, Y. Journaux and E. Pardo, *J. Am. Chem. Soc.*, 2012, **134**, 15301-15304.
- E. Coronado, M. Gimenez-Marques, G. M. Espallargas and L. Brammer, *Nat. Commun.*, 2012, **3**, ArtN 828.
- J. S. Costa, S. Rodriguez-Jimenez, G. A. Craig, B. Barth, C. M. Beavers, S. J. Teat and G. Aromi, *J. Am. Chem. Soc.*, 2014, **136**, 3869-3874.
- E. Coronado, M. Gimenez-Marques, G. M. Espallargas, F. Rey and I. J. Vitorica-Yrezabal, *J. Am. Chem. Soc.*, 2013, **135**, 15986-15989.
- E. Coronado, M. C. Gimenez-Lopez, G. Levchenko, F. M. Romero, V. Garcia-Baonza, A. Milner and M. Paz-Pasternak, *J. Am. Chem. Soc.*, 2005, **127**, 4580-4581.
- E. Coronado, M. C. Gimenez-Lopez, T. Korzeniak, G. Levchenko, F. M. Romero, A. Segura, V. Garcia-Baonza, J. C. Cezar, F. M. F. de Groot, A. Milner and M. Paz-Pasternak, *J. Am. Chem. Soc.*, 2008, **130**, 15519-15532.
- R. Yerushalmi, A. Scherz, M. E. van der Boom and H. B. Kraatz, *J. Mater. Chem.*, 2005, **15**, 4480-4487.
- A. A. Talin, A. Centrone, A. C. Ford, M. E. Foster, V. Stavila, P. Haney, R. A. Kinney, V. Szalai, F. El Gabaly, H. P. Yoon, F. Leonard and M. D. Allendorf, *Science*, 2014, **343**, 66-69.
- W. Fujita, K. Awaga, R. Kondo and S. Kagoshima, *J. Am. Chem. Soc.*, 2006, **128**, 6016-6017.
- M. Yamashita and H. E. Okamoto, *Material Designs and New Physical Properties in MX- and MMX-Chain Compounds*, Springer-Verlag Wien, 2013.
- E. Mateo-Marti, L. Welte, P. Amo-Ochoa, P. J. S. Miguel, J. Gomez-Herrero, J. A. Martin-Gago and F. Zamora, *Chem. Commun.*, 2008, 945-947.
- W.-W. Zhou, W. Zhao, X. Zhao, F.-W. Wang and B. Wei, *Synth. React. Inorg. Metal-Org. Nano-Met. Chem.*, 2013, **43**, 1171-1174.
- E. Cariati, D. Roberto, R. Ugo, P. C. Ford, S. Galli and A. Sironi, *Inorg. Chem.*, 2005, **44**, 4077-4085.
- E. Cariati, D. Roberto, R. Ugo, P. C. Ford, S. Galli and A. Sironi, *Chem. Mater.*, 2002, **14**, 5116-5123.
- F. Thébault, S. A. Barnett, A. J. Blake, C. Wilson, N. R. Champness and M. Schröder, *Inorg. Chem.*, 2006, **45**, 6179-6187.
- T. H. Kim, Y. W. Shin, J. S. Kim, S. S. Lee and J. Kim, *Inorg. Chem. Commun.*, 2007, **10**, 717-719.
- S.-M. Fang, Q. Zhang, M. Hu, B. Xiao, L.-M. Zhou, G.-H. Sun, L.-J. Gao, M. Du and C.-S. Liu, *Crystengcomm*, 2010, **12**, 2203-2212.
- R.-F. Song, Y.-B. Xie, J.-R. Li and X.-H. Bu, *Crystengcomm*, 2005, **7**, 249-254.
- Y. Takemura, T. Nakajima and T. Tanase, *Dalton Trans.*, 2009, 10231-10243.
- J. Bernasconi, P. Büesch, D. Kuse and H. R. Zeller, *J. Phys. Chem. Sol.*, 1974, **35**, 145-157.
- L. B. Coleman, M. J. Cohen, D. J. Sandman, F. G. Yamagishi, A. F. Garito and A. J. Heeger, *Sol. St. Commun.*, 1973, **12**, 1125-1132.
- J. Ferraris, D. O. Cowan, V. Walatka and J. H. Perlstein, *J. Am. Chem. Soc.*, 1973, **95**, 948-949.
- F. Wudl, G. M. Smith and E. J. Hufnagel, *J. Chem. Soc. D: Chem. Commun.*, 1970, 1453-1454.
- R. E. Peierls, *Quantum Theory of Solids*, Oxford University Press, Oxford, 1955.
- J. Troyano, J. Perles, P. Amo-Ochoa, J. I. Martinez, F. Zamora and S. Delgado, *Crystengcomm*, 2014, **16**, 8224-8231.
- R. A. Huggins, *Ionics*, 2002, **8**, 300-313.